The Journal of Chemical Physics

Density functional theory model study of size and structure effects on water dissociation by platinum nanoparticles

Cite as: J. Chem. Phys. **137**, 034701 (2012); https://doi.org/10.1063/1.4733984
Submitted: 16 April 2012 . Accepted: 21 June 2012 . Published Online: 17 July 2012

José L. C. Fajín, Albert Bruix, Maria Natália D. S. Cordeiro, José R. B. Gomes, and Francesc Illas


View Online

Export Citation

ARTICLES YOU MAY BE INTERESTED IN

A climbing image nudged elastic band method for finding saddle points and minimum energy paths
The Journal of Chemical Physics **113**, 9901 (2000); https://doi.org/10.1063/1.1329672

A consistent and accurate ab initio parametrization of density functional dispersion correction (DFT-D) for the 94 elements H-Pu
The Journal of Chemical Physics **132**, 154104 (2010); https://doi.org/10.1063/1.3382344

Modification of the surface electronic and chemical properties of Pt(111) by subsurface 3d transition metals
The Journal of Chemical Physics **120**, 10240 (2004); https://doi.org/10.1063/1.1737365

AIP Publishing

© 2012 American Institute of Physics.

Density functional theory model study of size and structure effects on water dissociation by platinum nanoparticles

José L. C. Fajín,[1] Albert Bruix,[2] Maria Natália D. S. Cordeiro,[1] José R. B. Gomes,[3,a)] and Francesc Illas[2,b)]
[1]*REQUIMTE, Faculdade de Ciências, Universidade do Porto, P-4169-007 Porto, Portugal*
[2]*Department de Química Física & Institut de Química Teòrica i Computacional (IQTCUB), Universitat de Barcelona, C/ Martí i Franquès 1, 08028 Barcelona, Spain*
[3]*CICECO, Departamento de Química, Universidade de Aveiro, 3810-193 Aveiro, Portugal*

(Received 16 April 2012; accepted 21 June 2012; published online 17 July 2012)

Size and structure effects on the homolytic water dissociation reaction mediated by Pt nanoparticles have been investigated through density functional theory calculations carried out on a series of cubooctahedral Pt_n nanoparticles of increasing sizes (n = 13, 19, 38, 55, 79, and 140). Water adsorption energy is not significantly influenced by the nanoparticle size. However, activation energy barrier strongly depends on the particle size. In general, the activation energy barrier increases with nanoparticles size, varying from 0.30 eV for Pt_{19} to 0.70 eV for Pt_{140}. For the largest particle the calculated barrier is very close to that predicted for water dissociation on Pt(111) (0.78 eV) even though the reaction mediated by the Pt nanoparticles involves adsorption sites not present on the extended surface. © *2012 American Institute of Physics*. [http://dx.doi.org/10.1063/1.4733984]

I. INTRODUCTION

Supported catalysts are constituted by an active phase, normally a metal, and a support, usually an oxide or a sulfide although inverse catalysts where oxide nanoparticles are dispersed on a metal support have been tested with success.[1] The effect of the metallic particle size on the performance of the catalysts for a given reaction is a hot topic that has been extensively studied in the past 20 years; especially after the finding by Haruta *et al.*[2] that nanosized Au nanoparticles supported on TiO_2 catalyze CO oxidation at temperatures as low as −70 °C. Chen and Goodman[3] suggested that the particle size effect is closely related to the concentration of irregularities in the catalyst surface, such as the presence of low coordinated atoms, which affect their catalytic performance. Size effects have also been found to be important in other catalyzed reactions, such as for instance, in the water gas shift (WGS) reaction ($CO + H_2O \rightarrow CO_2 + H_2$) on Cu and Au based catalysts.[4,5] Precisely, the WGS reaction is involved in industrial production of H_2 or in cleaning H_2 for subsequent use in fuel cells.[6–8] In industry, the WGS reaction is performed with catalysts in the form of Cu nanoparticles dispersed on a ZnO/Al_2O_3 support [see Refs. 9 and 10, and references therein]. However, supported Pt catalysts dispersed over various oxide supports such as Al_2O_3, CeO_2, ZrO_2, CeO_2–ZrO_2, and TiO_2 have received much interest during the last decade because of their WGS activity at low temperatures.[11–20] Platinum nanoparticles have also been recently proposed as catalysts for CO or CH_4 oxidation reactions.[21,22]

It is usually accepted that on metal supported catalysts the surface of the metal particle provides the active phase although there is also compelling evidence that other factors such as the nature of the support, the existence of point defects such as oxygen vacancies, the presence of promoters, or the catalyst preparation process, may significantly affect the catalytic activity and the overall catalyst performance.[23–26] In the case of the WGS reaction catalyzed by Pt particles deposited on ceria, an evident correlation between the particles size and the catalyst activity was found, although the interface between Pt and the support was also suggested to play an important role in the observed activity.[20] Likewise, Corma *et al.* have also shown that the catalytic activity of Au nanoparticles towards CO oxidation is enhanced when the particles are supported on nanostructured ceria.[27] However, it is not clear that the variation of catalytic activity with particle size arises solely from the presence of low coordinated sites. In fact, recent theoretical work shows that O_2 dissociation on Au nanoparticles is strongly affected by the particle size even when the reaction takes place at the same active site.[28,29]

Water dissociation is a simple chemical reaction but it takes part in several catalytic processes of industrial interest such as steam reforming of methanol ($CH_3OH + H_2O \rightarrow 3H_2 + CO_2$) and steam reforming of methane ($CH_4 + H_2O \rightarrow 3H_2 + CO$). It is also important for many other fields of chemistry such as corrosion, electrochemistry, or fuel cell technology and has been the object of several specialized reviews.[30,31] This simple reaction plays a dominant role in the molecular mechanism for the WGS reaction on metal-based catalysts.[32] In fact, this appears to be the rate limiting step for the different mechanisms proposed grouped in two main schemes termed *associative* and *redox* routes.[32] Recently, this elementary step has been investigated in a systematic way[33] for a rather large set of different planar and stepped transition metal surfaces and useful descriptors have been derived.[34]

a)Author to whom correspondence should be addressed. Electronic mail: jrgomes@ua.pt. Telephone: +351 234 401 423. Fax: +351 234 401 470.
b)Author to whom correspondence should be addressed. Electronic mail: francesc.illas@ub.edu. Telephone: +34 93 402 1229. Fax: +34 93 402 1231.

 © 2012 American Institute of Physics

In their systematic study, Fajín *et al.*[34] found that the activation energy barrier for water dissociation on the Pt(111) surface is moderately high, which seems to collide with the experimental evidences showing that supported Pt catalyst are active in the WGS reaction.[11–20] A possible explanation for this discrepancy is that, in addition to the role played by the underlying support, some specificity in the electronic structure of the metallic particles arising from the nanoscale size of the catalyst particles may play an important role here. In order to disentangle size and support effects and to contribute to the knowledge of the chemistry of Pt nanoparticles we have chosen to systematically study the effect of the particle size in the reaction of water dissociation mediated by models of platinum nanoparticles mimicking those observed in Pt supported catalysts and to compare the results with our recent findings for the same reaction on Pt(111), which has been studied using the same computational approach.[34] In addition, we aim to provide information about the scalability of the nanoparticles with respect to this elementary reaction. We recall that a change in trend with particle size may be expected to occur in the transition from so-called scalable to the non-scalable regime. For sufficiently large particles scaling relations can be applied to quantify how properties depend on particle size and approach the bulk limit, this is usually referred to as scalable regime.[35] On the contrary, for particles containing around 100 atoms or less, quantum effects dominate and can alter properties even with the smallest change; this is usually illustrated with the "every atom counts" statement.[36]

Finally, we attempt to rationalize the trends in adsorption energy and in activation energy for water dissociation with respect to the nanoparticles size. To this end we explore whether these quantities are in the scalable regime, as defined above, and also explore the applicability of the Brønsted-Evans-Polanyi (BEP) relationships[37,38] to rationalize the variation of the calculated energy profile with respect to particle size. The BEP relationships relating activation and reaction energy were initially introduced in an empirical way. Later on several studies provided a more solid basis[39–41] but it is perhaps after the work of Pallassana and Neurock[42] on ethylene hydrogenation and dehydrogenation on various metals surfaces that quantitative BEP relationships are established from density functional theory (DFT) calculations. These BEP relationships have been profusely used by Nørskov *et al.*[43] in many elementary reactions catalyzed by metal surfaces. Recent work, also by Nørskov *et al.*[44] has extended the applicability of BEP relationship to oxide surfaces as well. Therefore, it makes sense to investigate whether they do also hold when metallic nanoparticles, instead of extended surfaces, are involved in the reactions.

II. NANOPARTICLE MODELS AND COMPUTATIONAL DETAILS

Clusters containing 13, 19, 38, 55, 79, and 140 platinum atoms (denoted as Pt_{13}, Pt_{19}, Pt_{38}, Pt_{55}, Pt_{79} and Pt_{140}) constitute the models of Pt nanoparticles (NPs) considered in the present work. These NPs display regular cubooctahedral structure thus mimicking the shape of Pt nanocrystals often encountered in Pt supported catalyst and revealed by transmission electron microscopy (TEM) or its high-resolution variant (HRTEM) as illustrated in a feature article by Wang[45] and are similar to those introduced by Yudanov *et al.*[46] as models of single crystal surfaces and supported catalysts. The initial structures of the NPs are cut from bulk and their geometry fully relaxed. Each of the structures thus found was inserted at the center of a periodic box with a surrounding vacuum region of 10 Å to avoid the interaction with the neighboring nanoparticles artificially generated because of the use of a repeated unit cell approach. Except for the case of Pt_{13}, the structure predicted by geometry optimization is close to the starting one. The fact that for Pt_{13} the optimized structure significantly differs from the one cut from bulk indicates that this is more representative of a Pt small cluster than of a Pt nanoparticle. We note that these particular Pt NPs have been previously used to study the methane activation mechanism[47] and as support for carbon growth[48] and can be considered as reasonable models for the ones encountered in supported catalyst.

Total energy and structural parameters of adsorbed H_2O and co-adsorbed H and OH species as well the activation energy barrier for the adsorbed water dissociation reaction

$$H_2O\,^* + {}^* \rightarrow OH^* + H^*, \tag{1}$$

where * stands as usually for a free surface site, were determined through DFT-based calculations. In all cases, several different sites for the adsorption of the reactants and of the products on each of the nanoparticles were explicitly considered. This involves corner, edge, and terrace sites. Nevertheless, the interaction of these species with the low coordinate sites was always found to be the most favorable. This is not surprising and is in agreement with the behavior usually exhibited by stepped surfaces.[49,50] During the geometry optimization and transition state location calculations, the conjugate-gradient algorithm was used to allow a complete relaxation of the Pt atoms in the outermost layers of the Pt NPs, i.e., of those metal atoms directly interacting with the adsorbed species. Once the most stable sites were determined for reactants and products of the reaction described by Eq. (1), the transition state search was then performed by locating a saddle point that connects the most stable structure for the adsorbed H_2O molecule with the most stable structure for co-adsorbed OH and H species. The TS structure was then characterized by appropriate frequency analysis as indicated below and verifying that the imaginary frequency corresponds to the nuclear motion connecting reactants and products.

All DFT calculations were carried out using the VASP 4.6 computer code[51–53] and the PW91 form[54] of the generalized gradient approach (GGA) exchange-correlation potential. The valence density was expanded in a plane wave basis set with a cutoff of 415 eV for the kinetic energy of the plane waves. The projector augmented-wave (PAW) method[55] in the implementation of Kresse and Joubert[56] was used to take into account the effect of core electrons in the valence electron density and the calculations were carried out at the Γ point.

The choice of the PW91 potential follows from previous work exploring the performance of different exchange-correlation density functionals in the description of water dissociation on Cu(111) (Ref. 57) and of molecular oxygen

dissociation on Au NPs,[58] and has also been successfully used for the study of the complete WGS mechanisms on Pt(111) (Ref. 59) and on Cu(111).[32] It is also a common functional of choice for studying the reactivity of Pt nanoparticles.[48] Obviously, the calculated results will depend somewhat on the choice of the particular density functional method although there is strong evidence that calculated relative energies are much less affected than absolute energies by the GGA inherent errors.[49,60,61] Note that since the conclusions of the present work do not rely on the absolute value of the calculated adsorption, reaction, and activation energies but on the variation of the calculated values with respect to the NP size these will be less affected by the type of density functional. Another important issue concerns the possibility of spin-polarization. For a small Pt cluster such as Pt_8 it is found that the total magnetization of the lowest energy structure is 2 μ_B and there is a clear dependence between the atomic structure predicted by the calculation and the optimal number of unpaired electrons.[62] However, for larger nanoparticles, geometry optimization with spin-polarization either results in a closed shell state or the spin polarized solution has a total energy that is lower than that calculated for the closed shell configuration by a very small amount (of the order of 0.001 eV or less). This is in agreement with a recent systematic work carried out to explore the role of spin polarization in several reactions taking place at the surface of nonmagnetic metal surfaces.[63] In that work it was found that even for homolytic dissociation reactions at those metallic surfaces, spin polarized solutions exist although the total energy thus obtained is numerically very close to that corresponding to the spin restricted approach. Hence, all the calculations presented here have been performed with the spin restricted Kohn-Sham formalism.

The transition states (TS) on the different Pt NPs corresponding to the reaction described by Eq. (1) were located using the dimer approach.[64] Tight convergence criteria of 10^{-6} eV for the total energy change and 10^{-3} eV/Å for the forces acting on the relaxed atoms were always imposed; the same parameters were used for the convergence of the calculations aimed at providing energy and structure of adsorbed reactants and products. These quite strict criteria are necessary in TS searches and in the adsorption studies to avoid that the algorithm converges to spurious minima.

In order to find the optimum structures for isolated adsorbed water and for the co-adsorbed OH and of H species on the different Pt NPs, several different starting geometries and adsorption sites were considered as indicated schematically in Figure 1. The adsorption energies (E_{ads}) of H_2O and of the OH + H pair on the platinum nanoparticles were calculated as

$$E_{ads} = E_{NP-adsorbate} - E_{NP} - E_{H_2O}, \quad (2)$$

where E_{NP} refers to the total energy of the corresponding nanoparticle, E_{H_2O} refers to the total energy of a water molecule in the gas phase (computed by placing it in a sufficiently large box as required by the periodic cell approach), and $E_{NP-adsorbate}$ refers to the total energy of the nanoparticle-adsorbate system. Therefore, negative values of E_{ads} indicate favorable adsorption or co-adsorption.

The absence of imaginary frequencies in the pertinent analyses for the adsorbed reactants and products minimum energy structures ensured that those were true minima in the potential energy surface. Likewise, the presence of a single imaginary frequency for the configurations obtained with the Dimer method ensured that those structures were true transition states. The activation energy barrier, reaction energy, and adsorption energy values obtained were further corrected with the *zero point vibrational energy* (ZPVE) considering the standard harmonic oscillator approach.

The rate constants (k) at 463 K and at 573 K for the water dissociation elementary step at the Pt NPs mentioned above have been estimated from the transition state theory as follows:

$$k = \left(\frac{k_B T}{h}\right)\left(\frac{q^{\neq}}{q}\right) e^{\frac{-E_{act}}{k_B T}}, \quad (3)$$

where k_B is the Boltzmann constant, T is the absolute temperature, h is the Planck's constant, E_{act} is the activation energy from the ZPVE corrected calculated energy barrier and $q^{\neq}$ and q are the partition functions for the TS and initial state, respectively, which include vibrational terms only obtained from harmonic vibrational frequencies. For the initial state (IS) all normal modes of the H_2O molecule have been considered in the vibrational partition function whereas for the transition state (TS) all normal modes of the HO–H except for the one with an imaginary frequency were considered.

III. RESULTS

A. Structure and relative stability of reactants and products

First of all, a systematic series of calculations was carried out to determine the most stable mode and site for water adsorption as well as for OH + H co-adsorption on each nanoparticle. A summary of the results is given in Table I.[65] This table includes structural data and adsorption energies of the most stable adsorption sites found for each nanoparticle which in most situations involve adsorption on low coordinated metal atoms. In fact, adsorption at the corner sites of the nanoparticles was always found to lead to the most favorable interaction followed by the sites involving atoms at edges. Adsorption at the (111) terraces, exhibited by most of the nanoparticles considered in this paper, was found to be significantly less stable than on edge or corner sites and, as a result, geometry optimizations starting from the adsorbed species at these terraces usually converge to sites involving lower coordinated atoms which does not allow to study adsorption at these terrace sites. This is why Pt(111) is used to provide an adequate reference for large enough nanoparticles.

Water adsorption on the different Pt NPs follows a similar trend, water adsorbs through its oxygen atom on NPs top as in Figure 2, although the structure deformation induced by the presence of the adsorbate is always rather small. In any case the preference for the least coordinated top sites corroborates that, also for water adsorption on Pt NPs, the least coordinated atoms are also the most reactive as can be expected from previous work involving stepped surfaces.[33] Thus, it is

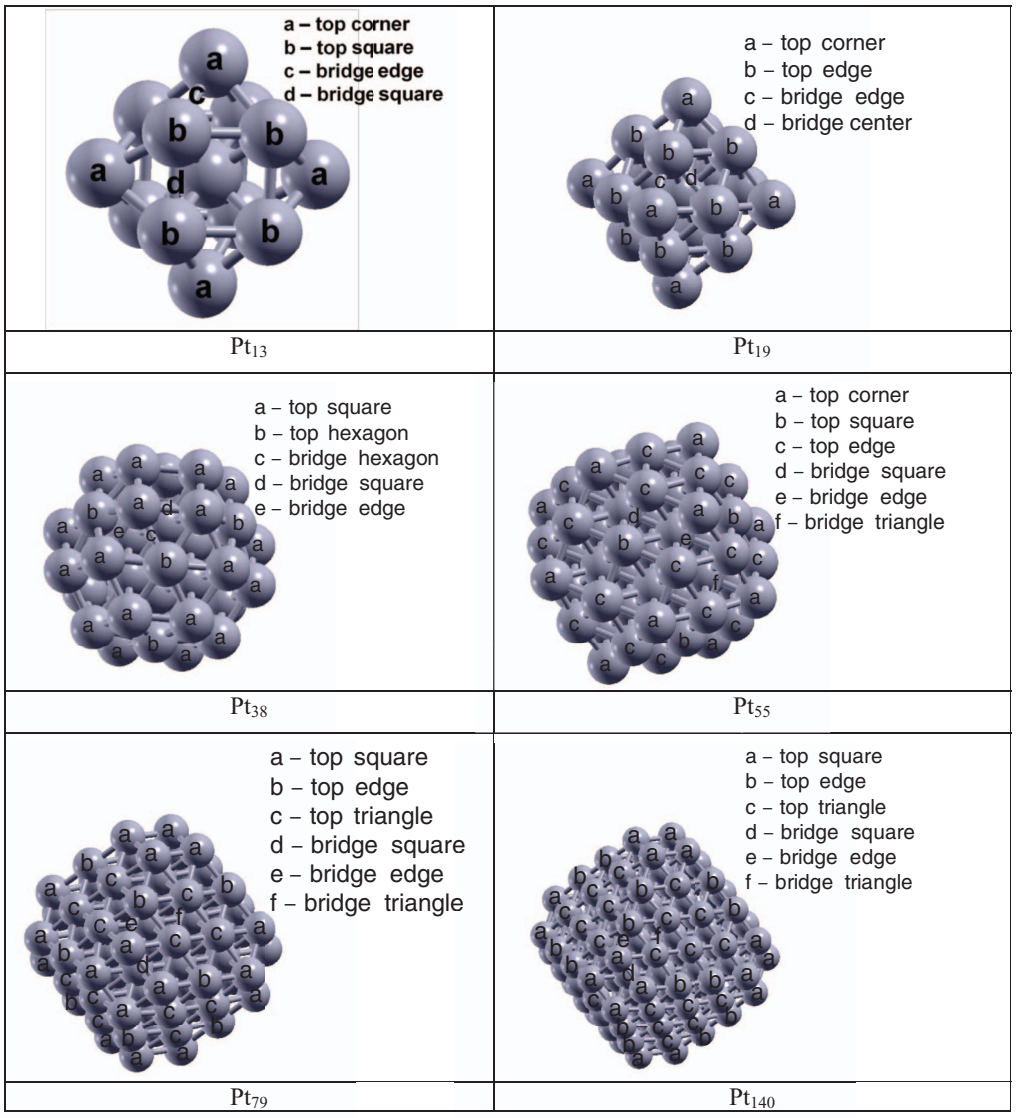

FIG. 1. Positions considered for H_2O and OH + H adsorption on the different platinum nanoparticles.

TABLE I. Adsorption energies and structural parameters for the most stable structures of water adsorbed and OH + H pair co-adsorbed on the platinum nanoparticles. Energy values are given in eV and distances in Å.

NP	Species	Position	E^{e}_{ads} [a]	E^{o}_{ads} [a]	$d_{O\text{-surf}}/d_{H\text{-surf}}$ [b]	$d_{O–H}$
Pt_{13}	H_2O	Top-corner	−0.58	−0.54	2.16	0.98; 0.98
	OH + H	Top-corner/bridge-edge	−0.90	−1.00	1.92/1.77; 1.73	0.98
Pt_{19}	H_2O	Top-corner	−0.50	−0.47	2.32	0.98; 0.98
	OH + H	Top-corner/top-edge	−0.66	−0.75	1.94/1.57	0.98
Pt_{38}	H_2O	Top-square	−0.52	−0.49	2.28	0.98; 0.98
	OH + H	Top-square/bridge-square	−0.41	−0.52	1.95/1.79; 1.76	0.98
Pt_{55}	H_2O	Top-corner	−0.62	−0.59	2.24	0.98; 0.98
	OH + H	Top-corner/bridge edge	−0.66	−0.76	1.94/1.73; 1.80	0.98
Pt_{79}	H_2O	Top-square	−0.53	−0.50	2.26	0.98; 0.98
	OH + H	Bridge-square/bridge-edge	−0.45	−0.54	2.13; 2.16/1.72; 1.78	0.98
Pt_{140}	H_2O	Top-square	−0.59	−0.55	2.26	0.98; 0.98
	OH + H	Bridge-square/bridge-edge	−0.46	−0.55	2.12; 2.15/1.70; 1.81	0.98
Pt(111)	H_2O	Top	−0.28	−0.27	2.51	0.98; 0.98
	OH + H	Bridge/hollow-fcc	0.49	0.39	2.18; 2.18/1.79; 1.89; 1.89	0.98

[a] In the adsorption energies (E_{ads}), the "e" and "o" labels stand for uncorrected and ZPVE corrected values, respectively.
[b] Distances corresponding to the dissociated H atom in the OH + H co-adsorption.

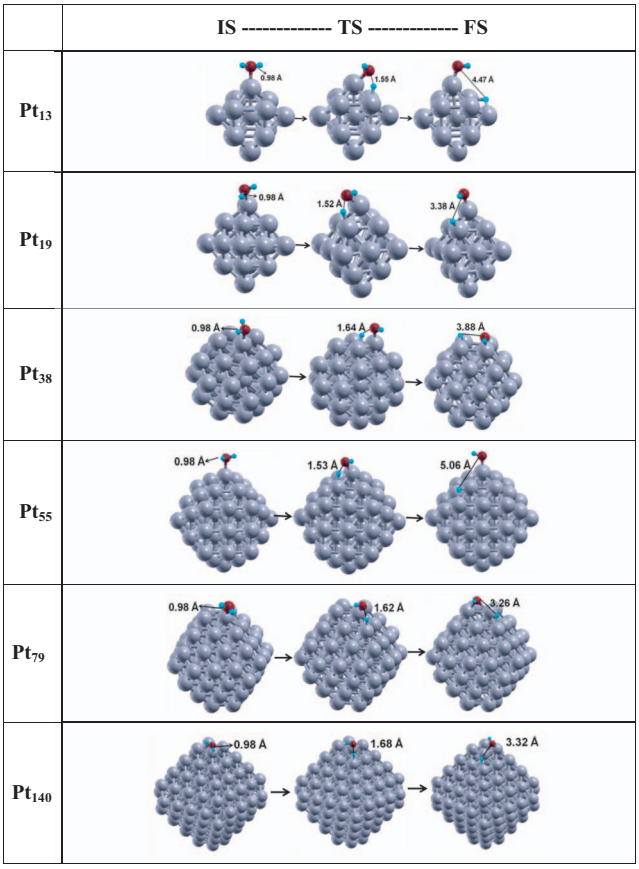

FIG. 2. Optimized structures for the initial (IS), transition (TS), and final (FS) states for the $H_2O^* + * \rightarrow OH^* + H^*$ reaction on the different platinum nanoparticles. Length of the cleaved O–H bond is given in Å.

found that water interacts more strongly with the top-corner sites in the Pt_{19} and in the Pt_{55} nanoparticles and with the top-square adsorption positions in the Pt_{38}, Pt_{79}, and in the Pt_{140} nanoparticles than with positions in the edges or in flat facets of the nanoparticles. Finally, the adsorption energy varies only in a modest way for different particle sizes with calculated values of −0.58, −0.47, −0.49, −0.59 −0.50, and −0.55 eV for Pt_{13}, Pt_{19}, Pt_{38}, Pt_{55}, Pt_{79}, and Pt_{140}, respectively. These values clearly indicate that the interaction of water molecules with the Pt NPs is rather local.

Next, let us consider the case of co-adsorption of OH and H on the different Pt nanoparticles which allows one to obtain the reaction energy for water dissociation reaction on these catalyst models. The adsorption energies for the OH + H pair, determined with respect to the energies of a water molecule in the gas phase and of the clean nanoparticle, are close to (for large NPs) or are more negative than (for small NPs) those corresponding to the water molecule adsorption on the same nanoparticles. This indicates that, depending on the NP, the reaction is exothermic or close to thermoneutrality while on the flat Pt(111) the reaction is clearly endothermic with a reaction energy of +0.66 eV.[34] It is also interesting to mention that OH is always more stable on top or bridge positions, depending on the nanoparticle considered, while H is more stable in bridge positions with the exception of the Pt_{19} nanoparticle where the most favorable configuration corresponds to H on the top site. One could argue that the size of the particle has less effect on water adsorption than on the adsorption energy of the final state (FS) or than on the activation energy. However, this is not due to particle size; it is due to the local structure of the different adsorbed species. In fact, the most stable adsorption site for H_2O on all the nanoparticles considered corresponds to a top-corner position or to the top-square adsorption positions (Table I and Figure 1). On the other hand, the structure of the FS and TS usually involves more than one Pt atom and the corresponding adsorption energy varies according to which atoms are involved (see also Table I and Figure 1). This is clear for the FS structures as one should note that OH and H preferentially adsorb on bridge-square/bridge-edge sites on Pt_{140} and Pt_{79}, with very similar adsorption energies of 0.46 and 0.45 eV, respectively. A similar situation appears for Pt_{19} and Pt_{55} which exhibit identical values for the adsorption energy of co-adsorbed OH and H. In this case the type of site where OH adsorbs is the same (a top-corner site) and even if the H atom occupies different sites (bridge and top, respectively), the same edge atom is involved. From the analysis of the different bonding modes of H_2O, OH, and H adsorbed on the Pt NPs it is possible to suggest three adsorption schemes: (i) adsorption on very small NPs such as the Pt_{13}, where adsorption induces a huge deformation of the NP, (ii) adsorption on NPs possessing top-corner sites, such as Pt_{19} and Pt_{55} NPs, and (iii) adsorption on NPs with exposed top-square positions such as in the cases of Pt_{38}, Pt_{79}, and Pt_{140} NPs.

B. Activation energy barrier and rate constant

In order to determine how the size of the Pt NPs affects the energy profile corresponding to the water dissociation reaction and, hence, their catalytic activity, we have studied the full reaction pathway starting always from the most stable adsorption position of the water molecule on each nanoparticle as described in Sec. III A. Once the TS that leads to OH + H co-adsorbed on the nanoparticle has been located and characterized, the activation energy barrier is determined as the energy difference between the TS and the starting point for the reaction (initial state or IS, which corresponds to the water molecule adsorbed on the NP); furthermore, the reaction energy was determined as the energy difference between the starting point and the final point of the reaction (final state or FS, which corresponds to the OH + H pair co-adsorbed on the corresponding NP). Table II reports this energy data as well as the length of the O–H bond which is being broken in the TS configuration. To better analyze the role of particle size, Table II also reports the transition state theory derived rate constants calculated at temperatures of 463 K and of 573 K, which are typical working temperature values for the WGS reaction[20,32] although it is clear that because of the simplicity of the models used the calculated values cannot be directly compared with experiment. A representation of the IS, TS, and FS for the most favorable reaction pathway for each of the Pt nanoparticles considered in the present work is reported in Figure 2. A comparison of the reaction profiles on the different nanoparticles is shown in Figure 3 whereas

TABLE II. DFT calculated parameters for water dissociation on several platinum nanoparticles.

Nanoparticle	O-H[a]	E_{act}^{e} [b]	E_{act}^{o} [b]	E_{react}^{e} [b]	E_{react}^{o} [b]	k (463 K/573 K)[c]
Pt_{13}	1.55	0.57	0.40	−0.32	−0.46	$7.34 \times 10^{7}/5.92 \times 10^{8}$
Pt_{19}	1.52	0.46	0.30	−0.17	−0.28	$1.61 \times 10^{8}/5.66 \times 10^{8}$
Pt_{38}	1.64	0.56	0.40	0.11	−0.03	$2.54 \times 10^{8}/2.10 \times 10^{9}$
Pt_{55}	1.53	0.74	0.57	−0.04	−0.17	$1.70 \times 10^{6}/3.16 \times 10^{7}$
Pt_{79}	1.62	0.64	0.48	0.08	−0.03	$3.73 \times 10^{6}/3.76 \times 10^{7}$
Pt_{140}	1.68	0.86	0.70	0.13	0.00	$2.30 \times 10^{4}/6.71 \times 10^{5}$
Pt(111)[d]	1.78	0.91	0.78	0.78	0.66	5.1×10^{3} /2.6×10^{5}

[a]HO-H breaking bond length in Å.
[b]In the activation (E_{act}) and in the reaction energies (E_{react}), the "e" and "o" labels stand for uncorrected and ZPVE corrected values, respectively.
[c]Reaction rate constants are given in s^{-1} at temperatures 463 K or 573 K.
[d]Results taken from Ref. 34.

Figure 4 reports the activation energy as a function of the number of atoms in the NP. The trend in Figure 4 is clearly nonmonotonic and rather oscillating suggesting that the set of nanoparticles under scrutiny is still on the non-scalable regime where every atom counts. The discussion in Sec. III C provides further support to this interpretation.

The calculated values for the activation energy barrier and for the adsorption energy on each nanoparticle suggest that only small nanoparticles could promote water dissociation in working conditions. In fact, the activation energy barriers for water dissociation on the Pt_{13}, Pt_{19}, and Pt_{38} are lower than the adsorption energy of the water molecule while in the case of the Pt_{55} and Pt_{79} NPs the activation energy barrier and the adsorption energy have similar values indicating that water dissociation will compete with water desorption (Figure 3). On the other hand, the activation energy barrier for water dissociation on the Pt_{140} is higher than the adsorption energy of the water molecule on that NP, which means that the reaction could only occur under special conditions of pressure and temperature. These findings are reminiscent of those reported in the work of Herzing *et al.* where it was suggested that only very small gold nanoparticles (∼0.5 nm or ∼10 atoms) were responsible for catalyzing the CO oxidation reaction on gold NPs supported on iron oxide.[66] Interestingly, the activation energy barrier for water dissociation on the largest Pt NP considered in this work is close to the activation energy barrier obtained for the same reaction on the Pt(111) surface,[34] suggesting that large platinum NPs have a reactivity similar to that of extended surfaces, at least for water dissociation.

From the preceding discussion one can conclude that the reactivity of the platinum nanoparticles towards water dissociation varies with the particle size. The activation energy barrier is strongly affected by the size of the nanoparticle. In fact, in the cases of the nanoparticles with 13, 19, and 38 Pt atoms, the stabilization of the TS is what leads to lower dissociation barriers with absolute values smaller than those corresponding to the adsorption energies of the water molecule on the same particles. These results are in concordance with the lower coordination of the Pt atoms in the active sites of small nanoparticles with respect to those at the surface of the larger nanoparticles. On the other hand, the adsorption energy of the water molecule is almost unaffected by the NP size, which contrasts with the results corresponding to the adsorption energy of the reaction products.

The calculated values for the water dissociation rate constants at 463 K and at 573 K are also given in Table II. In general, these values follow the sequence of values for the calculated activation energy barrier. Considering the values of k for the water dissociation calculated at different temperatures allows us to roughly estimate temperature effects even if one must realize that a direct comparison with experiment is yet not possible. From the calculated values for each NP one

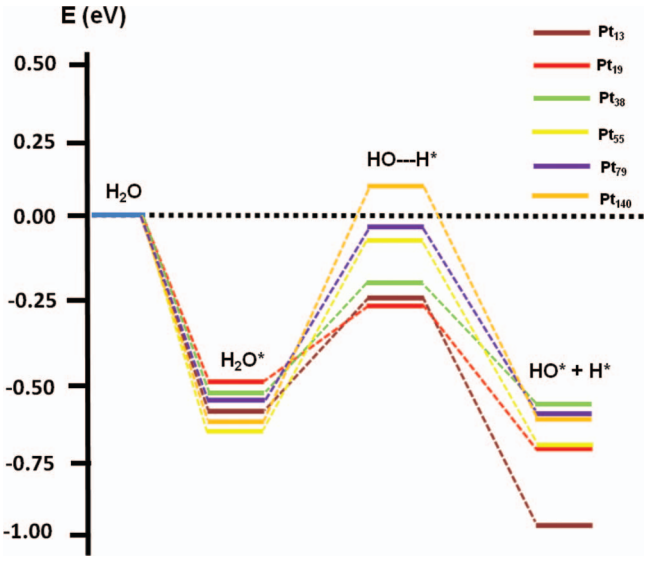

FIG. 3. Reaction profiles for the water dissociation on platinum nanoparticles.

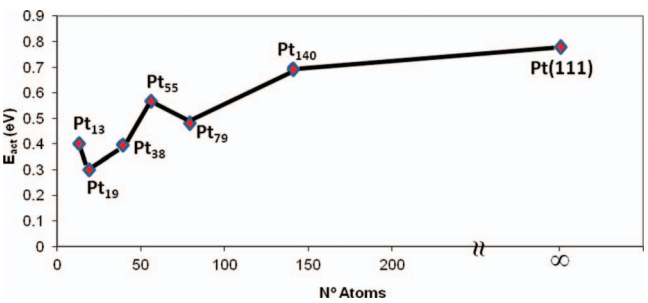

FIG. 4. Activation energy barrier with respect to the number of atoms in the Pt nanoparticles or extended (111) surface.

readily finds a difference of one order of magnitude between the k values at 463 K and 573 K.

Before closing this section it is worth to point out that for a comparison to water dissociation on real catalysts, the number of active sites in the nanoparticle also plays an important role in the activity of each of the nanoparticles considered. Thus, a more complete understanding of the activity of these nanoparticles towards H_2O dissociation should also consider the number of particles of each different size that can be generated with the same Pt loading and the number of active sites per particle. Also, discussing catalytic activity requires analyzing turn over frequencies or similar information. However, the main aim of this study is not the prediction of the catalytic activity of these particles towards water dissociation but the comparison of the potential energy surface for the dissociation of a single water molecule on a single site of a given nanoparticle. From a modeling point of view this allows us to investigate size and site effects on the potential energy surface without interference of other possible effects such as number or density of active sites.

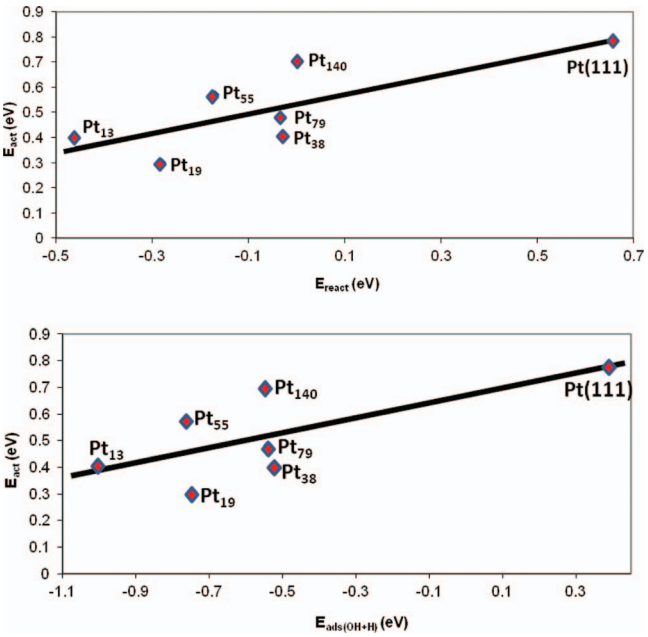

FIG. 5. Activation energy barriers with respect to the reaction energy (top) or with respect to the adsorption energy of the reaction products (bottom) for H_2O dissociation on Pt nanoparticles and on Pt(111) surface. Note that the black continuous line is just to guide the eye and does not represent a quantitative linear fit.

C. Brønsted-Evans-Polanyi Relationships

Here we will analyze whether BEP relationships can be derived for water dissociation by the model Pt NPs analyzed in this work. Nevertheless, one must caution that despite excellent BEP relations are obtained by mixing different kinds of reactions, substrates, and surface active sites,[67–69] it has been suggested that slightly better adjustments appear when making a distinction on reaction types,[69] the series of substrates,[70] or by differentiating pristine surfaces from defect sites.[67,71] These distinctions became critical in a recent study on the applicability of BEP relations on transition metal oxides surfaces.[44]

BEP relationships have been established for water dissociation on several transition metal surfaces.[34,72] In particular, previous work by Fajín *et al.*[34] reported three different relationships correlating the activation energy barrier with the reaction energy, with the adsorption energy of the reaction products, or with the adsorption energy of an oxygen atom. One must advert that these useful relationships have always been obtained for reactions taking place only at extended surfaces.[43,67–72] Therefore, we find it convenient to investigate whether these relationships can be generalized to the cases where the same chemical reaction is mediated by Pt NPs and whether Pt(111) can be considered as a particular case. To this end, the values corresponding to this extended surface have been included in the numerical derivation of these relationships which are displayed in Figure 5. In this figure is plotted the activation energy barrier either with respect to the reaction energy or with respect to the adsorption energy of the reaction products. The figure evidences a general trend but with a significant dispersion which does not allow one to obtain a quantitative correlation. The lack of correlation may originate from the still too limited size of the particles, which may be still below the scalable regime and it is thus not surprising to find that each one exhibits a particular chemical behavior given chemical particularity. To further investigate this hypothesis a series of analyses have been carried out which are described below.

Clearly, the observed behavior must have its origin in the electronic structure of the nanoparticles, we present an analysis of the projected density of states (pDOSs) to rationalize the differences observed in the reactivity of these nanoparticles. The pDOS has been obtained considering the atoms constituting the reaction sites and the plots for the initial, transition, and final states for H_2O dissociation on each nanoparticle and on the Pt(111) surface are shown in Figure 6. The overall shape and position of the bands of the pDOS is quite similar for all the cases studied although with significant differences in the intensity and number of peaks related to some of the bands. Therefore, a thorough analysis requires taking into account more subtle differences that allow rationalizing these plots, such as the shifts of the position of the valence bands. In the case of the extended metal surfaces it has been shown that for some reactions the role of the electronic structure can be reduced to a single parameter or descriptor, this is the so-called d-band model which correlates the adsorption energy with the position of the center of the metal surface d-band.[73] In those cases the BEP relationships are normally found to hold and, consequently, it is possible to relate the activation energy for a given elementary reaction taking place at a surface with the d-band center. The fact that the BEP relationships for H_2O dissociation by the Pt nanoparticles considered in the present work do not exhibit a quantitative linear behavior also implies that, at least for this reaction, the chemistry of these nanoparticles cannot be reduced to a single electronic structure parameter. In fact, the significant dispersion of points obtained when correlating the activation energy barriers and the adsorption energies of OH + H with

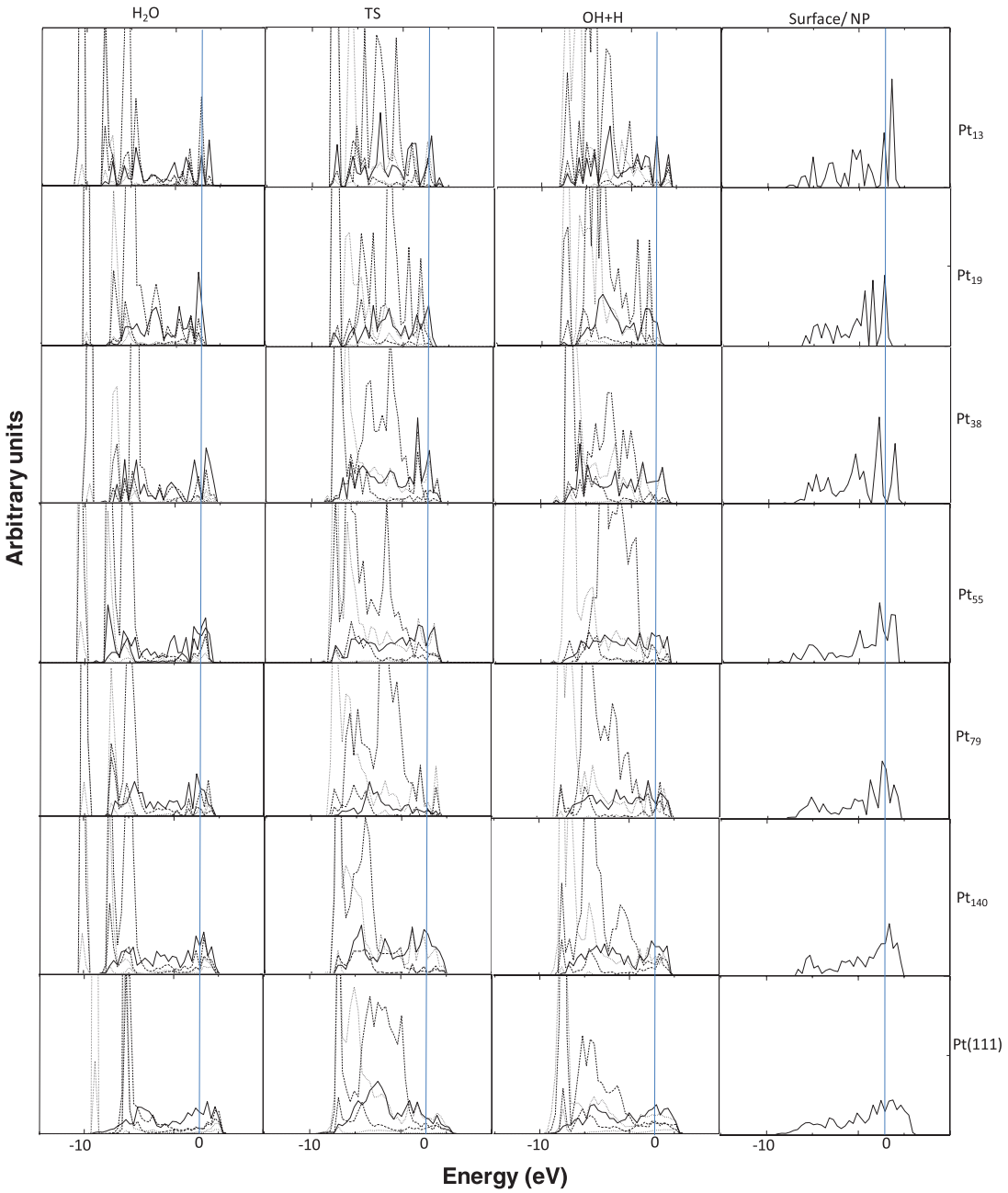

FIG. 6. Projected density of states (in arbitrary units) in front of energy relative to Fermi level (in eV) for the IS, TS, and FS corresponding to the most favorable reaction path for water dissociation on each Pt nanoparticle. The pDOS of the bare substrates is also represented in the rightmost panels. Dotted lines, dashed lines, and solid lines correspond to (s,p) bands of the H atoms, (s,p) bands of the O atom, and to the metal d bands, respectively.

the d-band center of the metallic substrates (Figure 7) shows that such a simple model does not hold, which is in agreement with the interpretation above regarding the fact that the particles considered, in particular, the smaller ones, are not yet in the scalable regime. This is further confirmed by the plot of the d-band center versus the surface to volume ratio in Figure 7(c) which is far from being linear. Note that the surface to volume ratio is given by $n^{-1/3}$; n being the number of atoms in the nanoparticle, and has been used to study the scalability of cohesive energies and structural features of metallic nanoparticles.[46,74,75] The lack of scalability has very recently been shown to be the cause for a nonlinear trend of the adsorption energy of CO on Pd nanoparticles with particle size.[76] One could argue that the BEP relations do not hold because the reaction does not evolve through exactly same reaction path. However, this is also the case for the extended surfaces, where BEP relationships exhibit a more quantitative linear behavior regardless of the structural differences between the reaction paths on the different metallic surfaces considered,[67–72] in particular for water dissociation on a broad range of metal surfaces.[34]

As already mentioned above, taking into account the structural peculiarities of H_2O, OH, and H adsorbed on the Pt NPs, it is possible to suggest three adsorption schemes, i.e., (i) adsorption on very small NPs such as the Pt_{13}, where adsorption induces a huge deformation of the NP, (ii) adsorption on NPs possessing top-corner sites, such as Pt_{19} and Pt_{55} NPs, and (iii) adsorption on NPs with exposed

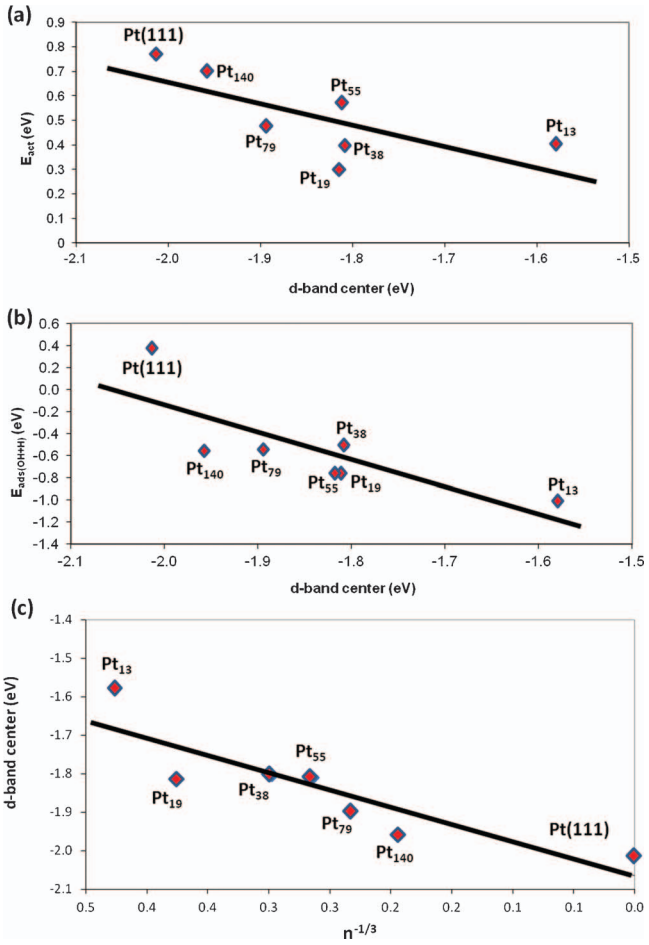

FIG. 7. (a) Activation energy barriers (E_{act}) and (b) adsorption energy of OH + H (E_{ads}(OH + H)) for water dissociation on several Pt nanoparticles and on the (111) surface with respect to the (local) d-band center (in eV) of the corresponding bare metallic substrate; and (c) d-band center respect to the inverse of the cubic root of the number of atoms on each NP.

top-square positions such as in the cases of Pt_{38}, Pt_{79}, and Pt_{140} NPs. Despite the consideration of a limited number of NPs in this work, the previous reasoning is compatible with the data points in Figure 5 (top).

A possible alternative interpretation can be tentatively inferred by further analyzing the data shown in Figure 5 (bottom). One could argue that the data points here correspond to two different BEP relations, one connecting Pt_{13}, Pt_{55}, and Pt_{140} and another one connecting Pt_{19}, Pt_{38}, and Pt(111). The two lines would have similar slopes but are separated by a constant offset. Such behavior has been previously observed when comparing flat and stepped metal surfaces. The offset has been interpreted as a result of a structural or geometric effect (flat terraces versus low coordinated sites), while the similar slope of both BEP lines would be related to an electronic effect.[43] However, even if this interpretation is really appealing, a closer inspection of the FS structures in Figure 2 does not fully support it. This is because for the Pt_{13} and Pt_{55} structures, the final state (OH* + H*), which is used as the x-axis descriptor in Figure 5, has OH* on a top site and H* on a bridge site whereas for Pt_{140} (and also for Pt_{79}) both OH* and H* are at a bridge position. The situation is similar for the Pt_{19}, Pt_{38}, and Pt(111) set. Pt_{19} and Pt_{38} do both have a FS with OH* on top sites and H* either at top (Pt_{19}) or bridge sites (Pt_{38}) whereas on Pt(111) the products are at different sites.

In any case, the previous analysis allows one to argue that the catalytic activity of transition metal nanoparticles is not only influenced by the effect of the particle size but also by the type of sites these nanoparticles exhibit which are relevant for the reaction of interest. This indicates that size and site effects are interrelated, a given particle size implies a type of site and, as a consequence, the BEP plots show a significant dispersion.

The above discussion allows one to suggest that the synthesis of transition metal nanoparticles with specific geometry can provide a tool for the rational design of catalysts with tailored properties.

IV. CONCLUSIONS

Density functional calculations within periodic approach and plane wave basis sets have been used to explore the nanoparticle size and structure effects in the water dissociation on various Pt nanoparticles containing up to 140 atoms. The chosen nanoparticle models have cubooctahedral structure and are denoted as Pt_{13}, Pt_{19}, Pt_{38}, Pt_{55}, Pt_{79}, and Pt_{140}. From the calculations concerning the determination of the most favorable dissociation pathway for the water dissociation on each nanoparticle, a series of general conclusions have been firmly established. Thus, the activation energy barrier for water dissociation on platinum nanoparticles and the adsorption energy of the reaction products depends markedly not only on the nanoparticle size but also on the type of site exhibited by the nanoparticles, whereas the adsorption energy of the water molecule does not present a clear dependence either on the size of the Pt nanoparticles or on their geometry. Likewise, a comparison between water adsorption energy and activation energy for water dissociation values for each nanoparticle leads to the conclusion that only small platinum nanoparticles are likely to promote water dissociation although it may be too speculative to extrapolate these conclusions to working conditions. Interestingly, water dissociation on Pt nanoparticles follows general BEP relationships similar to those previously derived for the same reaction on transition metal surfaces although the fitting is less quantitative. Finally, the catalytic activity of the larger platinum nanoparticle toward water dissociation is similar to that of extended surfaces. Therefore, results from the present study provide useful data for water dissociation mediated by Pt nanoparticles and it is likely that this may be also useful in the context of the WGS reaction.

ACKNOWLEDGMENTS

Financial support has been provided by Portuguese Fundação para a Ciência e Tecnologia (FCT), FEDER, and Programme Ciência 2007 (Grant Nos. PEst-C/EQB/LA0006/2011 to REQUIMTE and PEst-C/CTM/LA0011/2011 to CICECO and project PTDC/QUI-QUI/117439/2010 co-financed by Programa COMPETE), by Spanish MICINN grants FIS2008-02238 and, in part, by Generalitat de Catalunya (Grant Nos. 2009SGR1041

and XRQTC). J.L.C.F. acknowledges FCT for the grant SFRH/BPD/64566/2009 co-financed by the Fundo Social Europeu (FSE). A.B. acknowledges the Spanish MICINN for a predoctoral grant. F.I. acknowledges additional support through 2009 ICREA Academia award for excellence in research. Computational time has been generously provided by the Barcelona Supercomputing Centre through the HPC-Europa2 programme.

[1] J. A. Rodriguez, S. Ma, P. Liu, J. Hrbek, J. Evans, and M. Pérez, Science **318**, 1757 (2007).
[2] M. Haruta, N. Yamada, T. Kobayashi, and J. S. Iijima, J. Catal. **115**, 301 (1989).
[3] M. Chen and D. W. Goodman, Acc. Chem. Res. **39**, 739 (2006).
[4] J. A. Rodriguez, J. Evans, J. Graciani, J.-B. Park, P. Liu, J. Hrbek, and J. F. Sanz, J. Phys. Chem. C **113**, 7364 (2009).
[5] Q. Fu, H. Saltsburg, and M. Flytzani-Stephanopoulos, Science **301**, 935 (2003).
[6] A. Y. Rozovskii and G. I. Lin, Top. Catal. **22**, 137 (2003).
[7] M. A. Larrubia-Vargas, G. Busca, U. Costantino, F. Marmottini, T. Montanari, P. Patrono, F. Pinzari, and G. Ramis, J. Mol. Catal. A: Chem. **266**, 188 (2007).
[8] S. H. D. Lee, D. V. Applegate, S. Ahmed, S. G. Calderone, and T. L. Harvey, Int. J. Hydrogen Energy **30**, 829 (2005).
[9] C. V. Ovesen, B. S. Clausen, B. S. Hammershøi, G. Steffensen, T. Askgaard, I. Chorkendorff, J. K. Nørskov, P. B. Rasmussen, P. Stoltze, and P. J. Taylor, J. Catal. **158**, 170 (1996).
[10] N. Schumacher, A. Boisen, S. Dahl, A. A. Gokhale, S. Kandoi, L. C. Grabow, J. A. Dumesic, M. Mavrikakis, and I. Chorkendorff, J. Catal. **229**, 265 (2005).
[11] R. Burch, Phys. Chem. Chem. Phys. **8**, 5483 (2006)
[12] Y. Zhai, D. Pierre, R. Si, W. Deng, P. Ferrin, A. U. Nilekar, G. Peng, J. A. Herron, D. C. Bell, H. Saltsburg, M. Mavrikakis, and M. Flytzani-Stephanopoulos, Science **329**, 1633 (2010).
[13] G. Jacobs, L. Williams, U. Graham, G. A. Thomas, D. E. Sparks, and B. H. Davis, Appl. Catal. A: Gen. **252**, 107 (2003).
[14] T. Bunluesin, R. J. Gorte, and G. W. Graham, Appl. Catal. B: Environ. **15**, 107 (1998).
[15] A. A. Phatak, N. Koryabkina, S. Rai, J. L. Ratts, W. Ruettlinger, R. J. Farruto, G. E. Blau, W. N. Delgass, and F. H. Ribeiro, Catal. Today **123**, 224 (2007).
[16] H. Lida, K. Kondo, and A. Igarashi, Catal. Commun. **7**, 240 (2006).
[17] P. Panagiotopoulou, A. Christodoulakis, D. I. Kondarides, and S. Boghosian, J. Catal. **240**, 114 (2006).
[18] C. M. Kalamaras, I. D. Gonzalez, R. M. Navarro, J. L. G. Fierro, and A. M. Efstathiou, J. Phys. Chem. C **115**, 11595 (2011).
[19] I. D. Gonzalez, R. M. Navarro, W. Wen, N. Marinkovic, J. A. Rodriguez, F. Rosa, and J. L. G. Fierro, Catal. Today **149**, 372 (2010).
[20] C. M. Kalamaras, S. Americanou, and A. M. Efstathiou, J. Catal. **279**, 287 (2011).
[21] A. D. Allian, K. Takanabe, K. L. Fujdala, X. Hao, T. J. Truex, J. Cai, C. Buda, M. Neurock, and E. Iglesia, J. Am. Chem. Soc. **133**, 4498 (2011).
[22] Y.-H. Chin, C. Buda, M. Neurock, and E. Iglesia, J. Am. Chem. Soc. **133**, 15958 (2011).
[23] L. Li, Y. Zhan, Q. Zheng, Y. Zheng, X. Lin, D. Li, and J. Zhu, Catal. Lett. **118**, 91 (2007).
[24] H. Yahiro, K. Murawaki, K. Saiki, T. Yamamoto, and H. Yamaura, Catal. Today **126**, 436 (2007).
[25] J. A. Rodriguez, P. Liu, X. Wang, W. Wen, J. C. Hanson, J. Hrbek, M. Pérez, and J. Evans, Catal. Today **143**, 45 (2009).
[26] X. Wang, J. A. Rodriguez, J. C. Hanson, D. Gamarra, A. Martínez-Arias, and M. Fernández-García, J. Phys. Chem. B **110**, 428 (2006).
[27] S. Carrettin, P. Concepcion, A. Corma, J. M. L. Nieto, and V. F. Puntes, Angew. Chem. Int. Ed. **43**, 2538 (2004).
[28] A. Roldán, J. M. Ricart, and F. Illas, Theor. Chem. Acc. **128**, 675 (2011).
[29] A. Roldán, J. M. Ricart, F. Illas, and G. Pacchioni, Phys. Chem. Chem. Phys. **12**, 10723 (2010).
[30] P. A. Thiel and T. E. Madey, Surf. Sci. Rep. **7**, 211 (1987).
[31] M. A. Henderson, Surf. Sci. Rep. **46**, 1 (2002).
[32] A. A. Gokhale, J. A. Dumesic, and M. Mavrikakis, J. Am. Chem. Soc. **130**, 1402 (2008).
[33] J. L. C. Fajín, M. N. D. S. Cordeiro, F. Illas, and J. R. B. Gomes, J. Catal. **268**, 131 (2009).
[34] J. L. C. Fajín, M. N. D. S. Cordeiro, F. Illas, and J. R. B. Gomes, J. Catal. **276**, 92 (2010).
[35] I. V. Yudanov, A. Genest, and N. Rösch, J. Cluster Sci. **22**, 433 (2011)
[36] *Nanocatalysis*, edited by U. Heiz and U. Landman (Springer, Berlin, Germany, 2007).
[37] J. N. Brønsted, Chem. Rev. **5**, 231 (1928).
[38] M. G. Evans and M. Polanyi, Trans. Faraday Soc. **34**, 11 (1938).
[39] M. Kraus, Adv. Catal. **17**, 75 (1967).
[40] C. T. Campbell, J. M. Campbell, P. J. Dalton, F. C. Henn, J. A. Rodriguez, and S. G. Seimanides, J. Phys. Chem. **93**, 806 (1989).
[41] A. J. Gellman and Q. Dai, J. Am. Chem. Soc. **115**, 714 (1993).
[42] V. Pallassana and M. Neurock, J. Catal. **191**, 301 (2000).
[43] J. K. Nørskov, T. Bligaard, B. Hvolbæk, F. Abild-Pedersen, I. Chorkendorff, and C. H. Christensen, Chem. Soc. Rev. **37**, 2163 (2008).
[44] A. Vojvodic, F. Calle-Vallejo, W. Guo, S. Wang, A. Toftelund, F. Studt, J. I. Martínez, J. Shen, I. C. Man, J. Rossmeisl, T. Bligaard, J. K. Nørskov, and F. Abild-Pedersen, J. Chem. Phys. **134**, 244509 (2011).
[45] Z. L. Wang, J. Phys. Chem. B **104**, 1153 (2000).
[46] I. V. Yudanov, R. Sahnoun, K. M. Neyman, and N. Rösch, J. Chem. Phys. **117**, 9887 (2002).
[47] F. Viñes, Y. Lykhach, T. Staudt, M. P. A. Lorenz, C. Papp, H. P. Steinruck, J. Libuda, K. M. Neyman, and A. Gorling, Chem. Eur. J. **16**, 6530 (2010).
[48] F. Viñes, K. M. Neyman, and A. Goerling, J. Phys. Chem. A **113**, 11963 (2009).
[49] K. Honkala, A. Hellman, I. N. Remediakis, A. Logadottir, A. Carlsson, S. Dahl, C. H. Christensen, and J. K. Nørskov, Science **307**, 555 (2005).
[50] S. González, D. Loffreda, P. Sautet, and F. Illas, J. Phys. Chem. C **111**, 11376 (2007).
[51] G. Kresse and J. Hafner, Phys. Rev. B **47**, 558 (1993).
[52] G. Kresse and J. Furthmüller, Comput. Mater. Sci. **6**, 15 (1996).
[53] G. Kresse and J. Furthmüller, Phys. Rev. B **54**, 11169 (1996).
[54] J. P. Perdew, J. A. Chevary, S. H. Vosko, K. A. Jackson, M. R. Pederson, D. J. Singh, and C. Fiolhais, Phys. Rev. B **46**, 6671 (1992).
[55] P. E. Blöchl, Phys. Rev. B **50**, 17953 (1994).
[56] G. Kresse and D. Joubert, Phys. Rev. B **59**, 1758 (1999).
[57] J. L. C. Fajín, F. Illas, and J. R. B. Gomes, J. Chem. Phys. **130**, 224702 (2009).
[58] A. Roldán, J. M. Ricart, and F. Illas, Theor. Chem. Acc. **123**, 119 (2009).
[59] L. C. Grabow, A. A. Gokhale, S. T. Evans, J. A. Dumesic, and M. Mavrikakis, J. Phys. Chem. C **112**, 4608 (2008).
[60] C. H. Christensen and J. K. Nørskov, J. Chem. Phys. **128**, 182503 (2008).
[61] P. Strasser, Q. Fan, M. Devenney, W. H. Weinberg, P. Liu, and J. K. Nørskov, J. Phys. Chem. B **107**, 11013 (2003).
[62] A. Bruix, A. Migani, G. N. Vayssilov, K. M. Neyman, J. Libuda, and F. Illas, Phys. Chem. Chem. Phys. **13**, 11384 (2011).
[63] J. L. C. Fajín, M. N. D. S. Cordeiro, J. R. B. Gomes, and F. Illas, J. Chem. Theory Comput. **8**, 1737 (2012).
[64] G. Henkelman and H. Jónsson, J. Chem. Phys. **111**, 7010 (1999).
[65] Structural information regarding the Pt nanoparticles and the adsorption of H_2O and OH + H is available upon request to the authors.
[66] A. A. Herzing, C. J. Kiely, A. F. Carley, P. Landon, and G. J. Hutchings, Science **321**, 1331 (2008).
[67] J. K. Nørskov, T. Bligaard, A. Logadottir, S. Bahn, L. B. Hansen, M. Bollinger, H. Bengaard, B. Hammer, Z. Sljivancanin, M. Mavrikakis, Y. Xu, S. Dahl, and C. J. H. Jacobsen, J. Catal. **209**, 275 (2002).
[68] S. Wang, B. Temel, J. Shen, G. Jones, L. C. Grabow, F. Studt, T. Bligaard, F. Abild-Pedersen, C. H. Christensen, and J. K. Nørskov, Catal. Lett. **141**, 370 (2011).
[69] A. Michaelides, Z.-P. Liu, C. J. Zhang, A. Alavi, D. A. King, and P. Hu, J. Am. Chem. Soc. **125**, 3704 (2003).
[70] Z. P. Liu and P. Hu, J. Chem. Phys. **114**, 8244 (2001).
[71] A. Lagadottir, T. H. Rod, J. K. Nørskov, B. Hammer, S. Dahl, and C. J. H. Jacobsen, J. Catal. **197**, 229 (2001).
[72] A. A. Phatak, W. N. Delgass, F. H. Ribeiro, and W. F. Schneider, J. Phys. Chem. C **113**, 7269 (2009).
[73] M. Mavrikakis, B. Hammer, and J. K. Nørskov, Phys. Rev. Lett. **81**, 2819 (1998).
[74] A. Roldán, F. Viñes, F. Illas, J. M. Ricart, and K. M. Neyman, Theor. Chem. Acc. **120**, 565 (2008).
[75] F. Viñes, F. Illas, and K. M. Neyman, J. Phys. Chem. A **112**, 8911 (2008).
[76] I. V. Yudanov, A. Genest, S. Schauermann, H.-J. Freund, and N. Rösch, Nano Lett. **12**, 2134 (2012).